

# Aerothermal Analysis for the Mars Reconnaissance Orbiter

Michael A. Gallis, Wahid L. Hermina

*Sandia National Laboratories<sup>\*</sup>,*

*Engineering Sciences Center*

*Albuquerque, New Mexico*

Mark A. Johnson, Jim D. Chapel

*Lockheed Martin Corporation,*

*Space Exploration Systems*

*Denver, Colorado*

The force on and the heat flux to the NASA Mars Reconnaissance Orbiter (MRO) during drag passes are analyzed. Aerobraking takes place in the higher/rarefied levels of the Martian atmosphere, where traditional continuum fluid dynamics methods cannot be applied. Therefore, molecular gas dynamics simulations such as the Direct Simulation Monte Carlo Method are used to calculate these flow fields and provide heating and aerodynamic predictions for the vehicles. The heating and aerodynamic predictions calculated for the MRO include the heat transfer coefficient ( $C_h$ ), calculated for a number of angles of attack and the drag coefficient ( $C_D$ ) calculated for a number of altitudes and velocities. Bridging relations are sought that are applicable over the range of conditions of interest. A sensitivity analysis of the results to the chemical reaction rates, surface accommodation and temperature is also performed.

## Nomenclature

A	=	Cross sectional area ( $m^2$ )
AoA	=	Angle of attack (Deg)
$C_h$	=	Heat transfer coefficient $2q/(\rho U^3)$
$C_D$	=	Drag coefficient = $2F/(A \rho U^2)$
DSMC	=	Direct Simulation Monte Carlo
F	=	Total force (N)
HS	=	Hard sphere
Kn	=	System Knudsen number ( $\lambda/L$ )
kn	=	Local Knudsen number ( $\lambda/\Delta x$ )
L	=	Characteristic length (m)
U	=	Free stream velocity (m/s)
q	=	Heat flux ( $W/m^2$ )
VSS	=	Variable Soft Sphere

\* Sandia is a multiprogram laboratory operated by the Sandia Corporation, a Lockheed Martin Company, for the United States Department of Energy's National Nuclear Security Administration under contract DE-AC04-94AL85000.

Copyright © 2004, by Lockheed Martin Corporation. Published by the American Institute of Aeronautics and Astronautics, Inc. with permission.

VHS	=	Variable Hard Sphere
MRO	=	Mars Reconnaissance Orbiter
$T_w$	=	Wall temperature (K)

#### Greek

$\alpha$	=	Accommodation coefficient
$\Delta x$	=	Cell width (m)
$\lambda$	=	Mean free path (m)
$\rho$	=	Free stream density ( $\text{kg}/\text{m}^3$ )

## I. Introduction

The Mars Reconnaissance Orbiter (MRO), shown in Figure 1 (Lee et al.<sup>1</sup>) , scheduled for launch in 2005, will be equipped with cameras to zoom in for extreme close-up photography of the Martian surface, carry a sounder to find subsurface water and look for safe and scientifically worthy landing sites for future exploration. The MRO will also establish a crucial service for future spacecraft, to becoming the first relay station for future missions to Mars. The MRO will be the first link in a communications bridge back to Earth to be used by numerous spacecraft in coming years. In addition, the mission will also includes an experimental optical navigation camera that will demonstrate a new method for determining spacecraft position and velocity as the MRO approaches Mars.

After traveling for seven months, the MRO is expected to reach Mars and place itself in a highly elliptic orbit around it with the aerobraking phase beginning shortly after that. From then on, flight team members still have six months to slow the spacecraft down and bring it into a near-circular science-mapping orbit (255-320 km). Using atmospheric drag to aerobrake, the MRO will dip into the Martian atmosphere once every time it swings by its closest approach to Mars (periapsis).

Aerobraking is a technique that has been used in interplanetary missions to reduce fuel requirements during orbit-placing maneuvers. The purpose of drag passes is to use atmospheric drag instead of retrograde thrusters to provide the necessary drag to modify the orbit of the vehicle to the desired one. However, aerobraking introduces its own risks and difficulties. During the aerobraking maneuvers, the vehicle should be aerodynamically stable, and its thermal load cannot exceed the maximum allowed values for each particular component. To accurately model the complex behavior during aerobraking, the thermal analysis must be coupled to the three-dimensional, time-varying aerodynamic analysis.

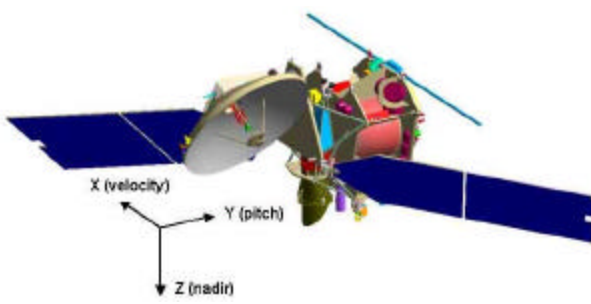


**Figure 1.** MRO Spacecraft Configuration in the Primary Science Orbit

Although aerobraking takes place at the point of closest approach to the planet, the atmospheric densities encountered place the flight of the vehicle near the free molecular regime. For the particular case of the MRO, a typical mean free path during aerobraking is almost 1m and the characteristic Knudsen number, defined as  $\text{Kn} = \lambda/L$ , has a typical value of at least of 0.5, which clearly places the aerobraking maneuver in the regime of rarefied aerodynamics.

The analysis in the following sections focuses on two parameters of interest to the designers: the heat transfer coefficient and the drag coefficient. In this first part of the analysis, the effects of different angles of attack and different flight altitudes are examined. The second part of the analysis deals with the sensitivity of the results to the simulation parameters. More specifically, the effects of the uncertainty in chemical reaction rates, surface temperature, and finally accommodation coefficient on the heat flux to the MRO are examined.

## II. Methodology Used

The Direct Simulation Monte Carlo (DSMC) method of Bird<sup>2</sup> is currently the most popular numerical method for the study of hypersonic rarefied aerodynamics. Based on an algorithm developed by G.A. Bird of the University of Sydney in 1960, DSMC calculates the molecular collisions using stochastic rather than deterministic procedures. The computational efficiency of DSMC compared to other particulate methods (such as Molecular Dynamics) is such that today DSMC is almost universally used in the area of rarefied gas dynamics, or where mean free path phenomena are of interest.

In the DSMC methodology, a gas flow is represented by the motion of a number of “computational molecules,” each of which represents a large number of real molecules. A computational molecule travels at constant velocity until it experiences a collision with another computational molecule or a boundary. Collisions are binary and change the velocities and the internal energies but not the positions of the colliding pair of computational molecules. It should be noted that computational molecules have three-dimensional velocity vectors for collision purposes, regardless of the dimensionality of the geometry. The result of this approach is a statistical, physical simulation of the dynamics and interactions of millions and in some cases billions of gas molecules.

There are several choices of collision models that can be used. These include the Hard Sphere (HS), Variable Hard Sphere (VHS), and Variable Soft Sphere (VSS) models. The HS model is capable of matching the viscosity of a gas at only one temperature, the VHS model matches the temperature-dependent viscosity of a gas, and the VSS model matches the temperature-dependent viscosity and self-diffusion coefficient of a gas.

Computational molecules travel at constant velocity for the entire time step or until a boundary is encountered (move phase). In the latter situation, the appropriate boundary condition is applied. Typical boundary conditions are “inflow” (computational molecules enter the domain with a prescribed Maxwellian distribution), “outflow” (computational molecules crossing this boundary are deleted, appropriate for supersonic applications), “diffuse wall” (computational molecules are reflected usually with a prescribed Maxwellian distribution), and “specular wall” (computational molecules are reflected with mirror symmetry).

A computational mesh is used in the DSMC method for identifying possible collision partners and to accumulate statistical information. Moments of the molecular velocity distribution function are accumulated over one or more time steps within each mesh cell to yield gas quantities such as the number density, velocity and temperature. Forces on molecules, such as gravity or electrostatic forces for ions can be incorporated. To preclude non-physical behavior, time steps and mesh cells are constrained to be less than about one-third of a collision time and one-third of a mean free path, respectively.

For the purposes of this work the “DAC” DSMC implementation of LeBeau<sup>3</sup> was used. Since the DSMC algorithm is well established on physical arguments, DSMC implementations differ mostly in the flow field discretization methods and the way they represent the geometry modeled. The DAC software employs a two-level embedded Cartesian grid system. Thus the computational domain is a rectangular box, aligned with the Cartesian axes. Embedded within the flow field grid is the surface geometry. DAC represents the surface geometry as a collection of unstructured triangular elements, which also act as sampling zones for surface properties.

The rectangular bounding box for the computational domain is specified by the user, as is the discretization in each of the three Cartesian directions. The cells created by this uniform Cartesian grid are referred to as Level-I Cartesian cells. Each of these Level-I Cartesian cells can be further refined by its own embedded Cartesian grid. These embedded Cartesian grids form Level-II Cartesian cells. The two-level embedded Cartesian grid system permits variable refinement throughout the computational domain, which is essential for meeting the local mean-free-path cell size requirement.

To model chemical reactions Bird’s Total Collision Energy (TCE) model was used. The chemical reaction data used in the simulations are those proposed by Park.<sup>4</sup>

## III. Model Development

The model of the MRO was based on a CAD design provided by mission designers. From this model three surface grids were created with  $0.5 \times 10^5$ ,  $1 \times 10^5$  and  $2 \times 10^5$  surface elements. The three surface grids were used to evaluate the convergence of the sensitivity of the surface properties to grid resolution. A preliminary analysis was done where 6 combinations of surface and gas phase grids were used. For the preliminary analysis the gas phase grids were not adapted. The surface and gas -phase grid combinations are given in Table 1.

<i>Surface cells</i>	50,000	100,000	200,000
<i>Gas-phase cells</i>			
200,000	Case 1	Case 3	Case 5
1,000,000	Case 2	Case 4	Case 6

**Table 1.** Preliminary cases

The calculated  $C_h$  coefficients are shown in figures A1-A6 in the Appendix. From these figures, it is seen that from the coarsest case (case 1) to the finest case (case 6) the values of  $C_h$  do not change significantly. Some differences near the edges of the solar panels can be attributed to edge effects, where local flow gradients must be captured by the gas phase grid. As a result, it was concluded that the finest possible initial configuration was to be used, i.e.  $2 \times 10^5$  surface cells and  $1 \times 10^6$  gas-phase cells. With this configuration, the cell sizes were about 10% of the free stream mean free path, a very conservative choice for a DSMC simulation. As will be shown in the following sections, the mesh adaptation process will increase the gas -phase cells to more than double the number of cells. However, the mesh adaptation process cannot change the number of surface cells.

#### IV. Grid Adaptation Process

For the gas-phase grid adaptation, the “Level-II cell” procedure (outlined in the following section) was used. Since the size of the initial cells was already 10% of the free stream mean free path, the need to adapt the mesh was expected to be limited and necessary only near the surface to capture the compression layer that developed.

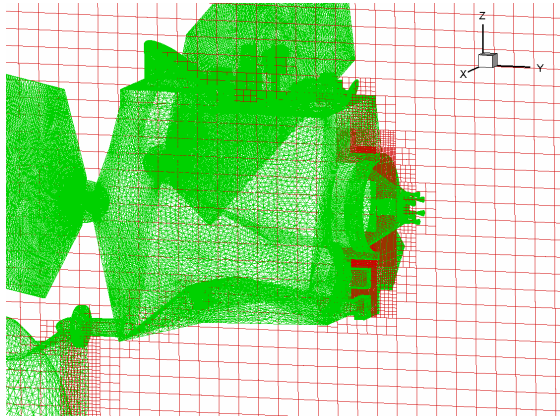


**Figure 2.** Gas phase grid (adapted)

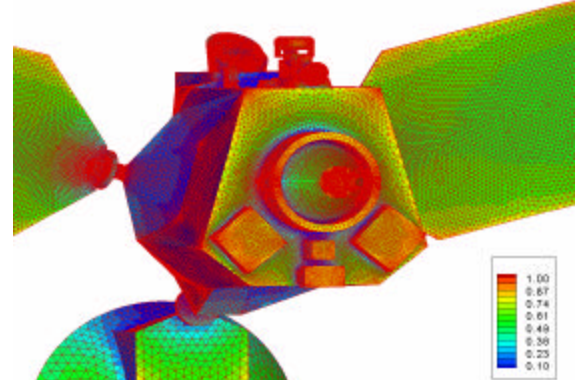


**Figure 3.** Detail of surface grid ( $C_h$  in the background)

The adaptation procedure was allowed up to 100 Level-II cells in each Level-I cell, which was a very generous setting since it was never used. However, the fact that the adaptation procedure matched the local refinement criterion of sub-mean free path cells without exceeding its size limitation is yet another indication that the grid produced was refined enough.

The final grid (shown in Figure 2) used about  $2 \times 10^6$  cells, while the triangular surface grid as noted earlier used  $2 \times 10^5$  surface elements (shown here in figure 3). Since the adaptation procedure does not allow adaptation of the surface grid,  $2 \times 10^5$  cell surface grid was used to ensure that surface properties were adequately resolved. It can be seen in Figure 3 that most of the cells were concentrated around the instrumentation.

## V. Simulation Details

Grid resolution is not the only critical aspect to a DSMC simulation. The number of computational molecules, the time step, and the steady-state time are other parameters that can influence the quality of a calculation. Table 2 presents typical values of these parameters for the simulations performed. Every possible effort was made to ensure that all these parameters complied with Bird's criteria<sup>2</sup> for a successful DSMC simulation. The time step was such that molecules, on average, did not move more than a third of a cell per time step and cells were smaller than the local mean free path .

<i>Simulation Parameter</i>	<i>Numerical Value</i>
Moves to steady state	5000
Total number of moves	$(0.5-1) \times 10^5$
Number of simulators	$20 \times 10^6$
Number of simulators per cell	10
Total number of cells (LI & LII)	$2 \times 10^6$
Number of grid adaptations	1

**Table 2.** Typical simulation parameters

The calculations were performed on two SGI-R10000 Origin platforms with 32 and 64 processors each. Calculations typically took 3-5 days and used 16-32 processors depending on the computational load of the case.

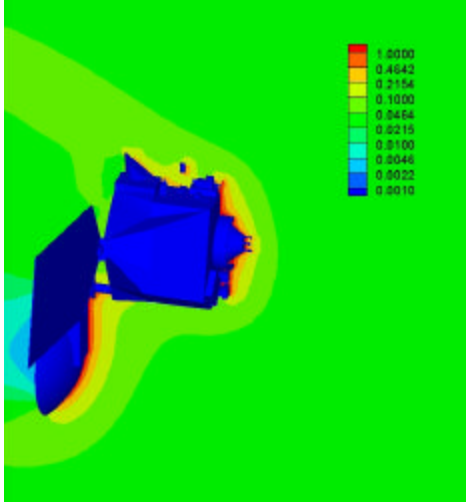


**Figure 4.** Number density profile

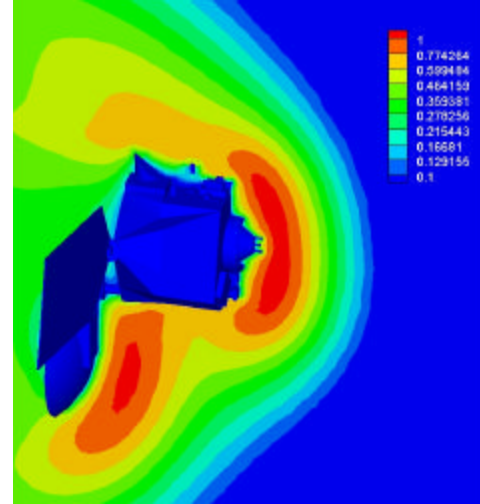


**Figure 5.** Translational temperature

Each of these simulations was executed for about  $5 \times 10^4 - 1 \times 10^5$  steady state moves, taking a sample of the flow field after every move. Taking into consideration that each particle takes 3 moves to change cell location, probably about a third of the  $5 \times 10^4 - 1 \times 10^5$  samples are independent. This would lead to a statistical error for the simulation of about 1%. It must be stressed however that statistical error is not the only source of error in these simulations. As will be discussed later, error is introduced in the calculations through uncertainties in the chemical-reaction-rate data and the surface accommodation coefficients that are not known to within 1% accuracy.

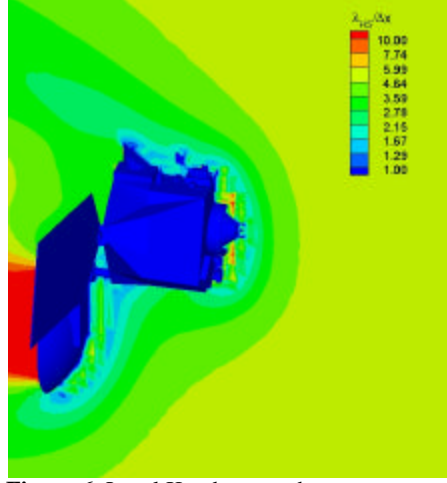


**Figure 6.** Local Knudsen number

Figures 4 and 5 present the normalized (by their maximum values) translational temperature and density profiles for a nominal aerobraking case. The flow comes from right to left. The density profiles of Figure 5 show an increase of two orders of magnitude in an extended compression layer in front of the MRO. As mentioned in the introduction, the density and the collisionality of the flows considered herein are low and not capable of establishing a distinct shock layer. Due to the density gradient, molecules diffuse from the compression layer upstream and collide with the incoming free stream molecules, creating a layer where the temperature rises to about 1.0 (Figure 4). The density and temperature drop in the wake of the MRO due to the rapid expansion.

Figure 6 shows the local Kn number for this flow field. The local Knudsen number (kn) has a value greater than 1. everywhere in the domain. A value of 1.0 is a minimum for a physically realistic DSMC simulation

#### A. Effect of the Angle of Attack on the Heat Transfer Coefficient

In the first part of the investigation the effect of the angle of attack on the heat flux to the vehicle was considered. Since the purpose of aerobraking is to reduce the velocity and the altitude of the vehicle, every pass takes place with different conditions (velocity and free stream density). To simplify the analysis, all the results will be presented normalized by their maximum values.

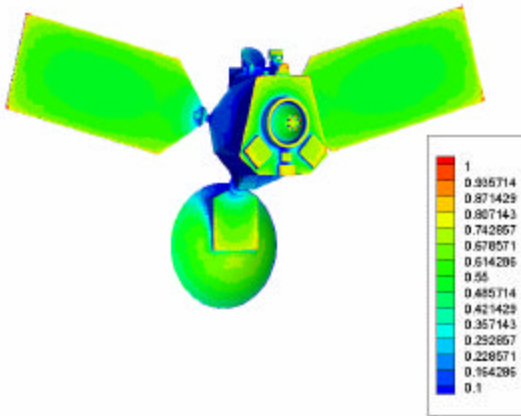


**Figure 7.**  $C_h$  for nominal aerobraking conditions

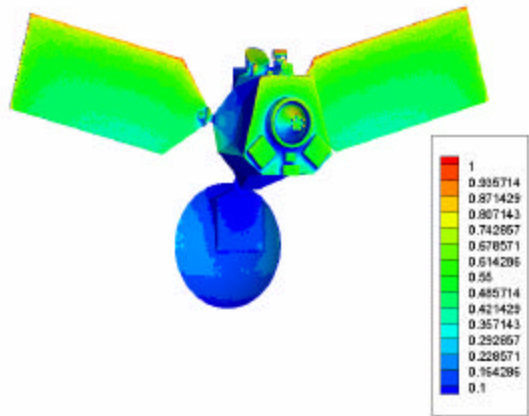


**Figure 8.**  $C_h$  when aerobraking at a positive AoA

Depending on the angle of attack, the maximum heating points move along the surface of the MRO. However, it should be noted that in all cases the edges of the solar panels appear to be more exposed to the flow, allowing the heat transfer there to reach maximum. The reason for this is that the solar panels are located in the wake of the shock caused by the main body of the MRO. Results for some of these cases are given in Figures 7 to 10.

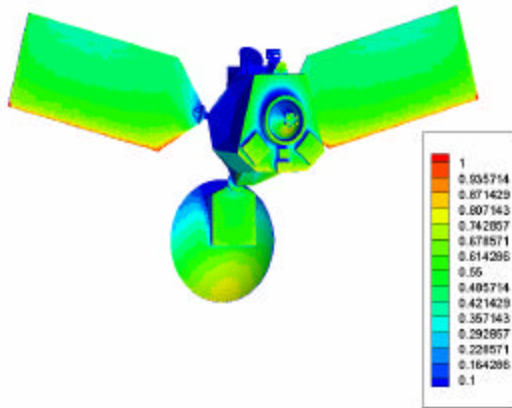


**Figure 9.**  $C_h$  when aerobraking at a negative AoA

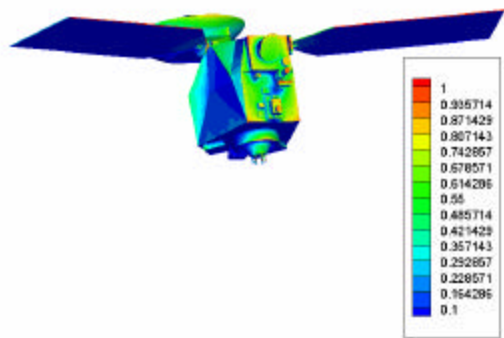


**Figure 10.**  $C_h$  for anomalous aerobraking with science instruments head on into the flow

Apart from the edges of the solar panels, the heat flux coefficient does not change significantly and has an average value of about 0.7 in the middle of the panels. Near the edges, and in particular at the corners, the heat transfer coefficient reaches a value of almost 1.0, indicating that these are the most sensitive areas of the MRO.

The instruments on top of the vehicle are well protected in the case of zero angle of attack (nominal conditions), because they are downstream of the shock where the energy content of the flow is lower due to chemical reactions. It should be remembered<sup>5</sup> that most chemical reactions that take place in these flow fields are endothermic dissociation reactions. In the case of a positive angle of attack, these instruments are exposed to the free stream flow and therefore to a higher heat flux.

## B. Effect of Chemical Reaction Rates

One of the most significant problems in hypersonic aerodynamics is the prediction of non equilibrium chemical reactions in the flow field. The chemistry model for this study uses as input measured or calculated equilibrium reaction rates to estimate the reaction probability under non equilibrium conditions. Evidently, the method is sensitive to its input: *the equilibrium reaction rates*. Measurements at temperatures in excess of 10,000 K are almost impossible to do, and molecular-beam experiments are very rare for the species and reactions of interest. The chemical reaction rates are usually measured at lower temperatures and then the reaction rates are extrapolated to higher temperatures. This way another source of error is introduced: *the uncertainty of the equilibrium chemical reaction rates*.

To assess the effect of chemical reaction rates and the sensitivity of the flow field to these rates, two cases were examined. The conditions of both cases correspond to the nominal aerobraking case. In the first one, the CO<sub>2</sub> dissociation rate was reduced by one order of magnitude and in the second one it was increased by one order of magnitude. Dissociation of CO<sub>2</sub> is the main reaction that takes place in the flow field<sup>4</sup> that could have an impact to energy content of the flow due to its significant energy threshold. The heat transfer coefficients are shown in Figures 11 and 12.

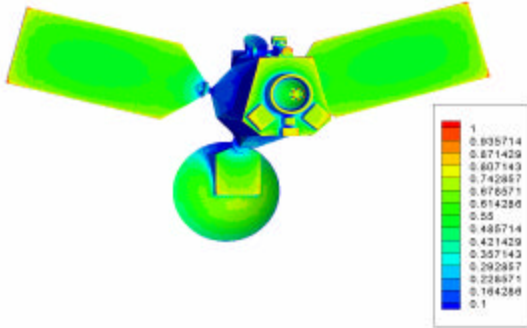


**Figure 11.**  $C_h$  for reduced reaction rates

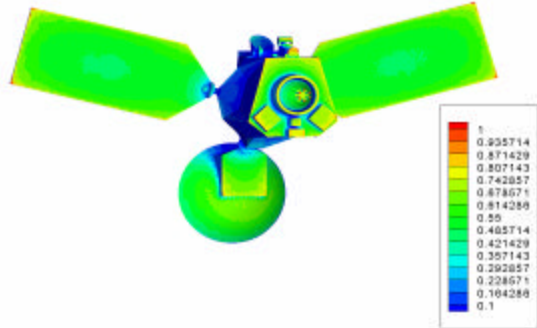


**Figure 12.**  $C_h$  for enhanced reaction rates

As expected in the second case where the rates were stronger, more  $\text{CO}_2$  dissociates reducing the energy content of the flow impinging on the MRO. As would be expected this case presents a 50% reduction of the heat flux in the middle of the solar panels. However, the first case, which is the worst-case scenario, did not show significant differences. This is due to the small collisionality of the flow, which makes chemical reactions infrequent.

### C. Effect of Wall Temperature

The wall temperature can, to some extent, influence the flow. Molecules reflected off the surface are accommodated fully or partially, altering the energy content of the compression layer near the surface. To assess these effects, calculations were executed with wall temperatures ranging from 25 K to 300 K.

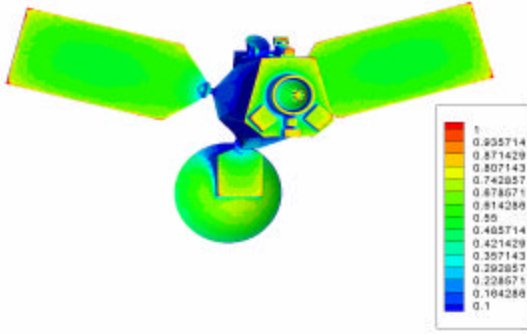


**Figure 13.**  $C_h$  for  $T_w = 25 \text{ K}$

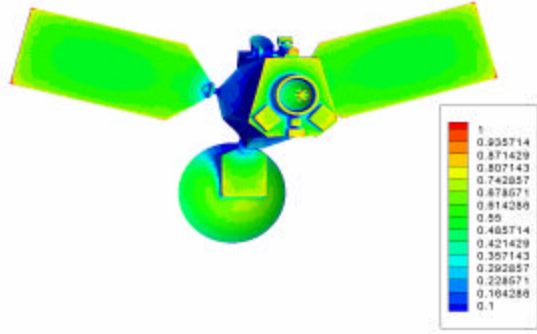


**Figure 14.**  $C_h$  for  $T_w = 300 \text{ K}$

The results from two of these calculations are shown in figures 13 and 14 for a wall temperature of 25K and + 300K, respectively. The effect of the wall temperature is seen to be negligible. This is due to the high energy content of the incoming flow that is the dominant contribution to the energy content of the compression layer.

### D. Effect of Accommodation Coefficient

Engineering surfaces are known to have thermal accommodation coefficients close to unity. However, prolonged exposure to a near-vacuum environment can reduce the level of molecular thermal accommodation.

All calculations presented here used an accommodation coefficient of 1.0. To assess the effect of a reduced accommodation coefficient, two more calculations with a more realistic accommodation coefficient of 95 and 85% were performed.

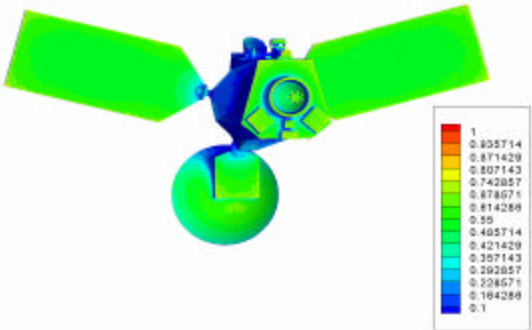


**Figure 15.**  $C_h$  for  $\alpha = 95\%$

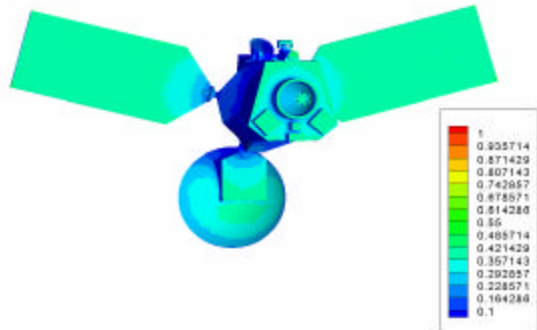


**Figure 16.**  $C_h$  for  $\alpha = 85\%$

The results of these simulations are given in Figures 15 and 16, and as expected, for this near-free-molecular case, reducing the accommodation coefficient reduces the heat flux coefficient. In a perfectly free-molecular case, the heat flux coefficient is linearly proportional to the accommodation coefficient. Even a limited number of collisions can offer a “shielding effect” that skews this relationship by increasing the time molecules spend close to the surface, therefore increasing the probability of an energy exchanging reaction in the gas-phase.

#### E. Drag Coefficient During Drag Passes at Different Altitudes

As noted in the introduction, every aerobraking pass will reduce the speed of the MRO, therefore reducing the flight altitude. To predict the behavior of the orbiter during these passes, the drag coefficient needs to be calculated for a number of altitudes and flight conditions. Figure 17 presents the drag coefficient for these cases and two numerical fits to the data.

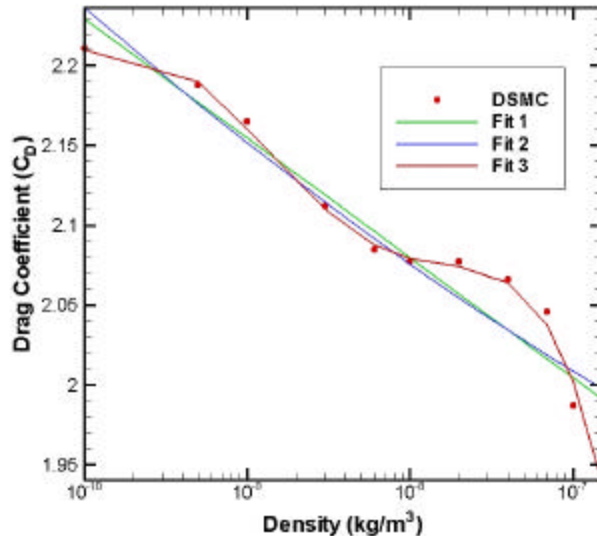


**Figure 17.** Drag coefficient

The curve designated as “Fit 1” is given by  $1.47952 - 0.032578 \log(\rho)$  and Fit 2 by  $1.79032 + 8.41026 (\log(\rho))^2$ . Higher order functions (such as Fit 3 which is an 8<sup>th</sup>-order fit) can approximate the DSMC points more accurately. Similar fits were produced by Wilmoth<sup>6</sup> for the Viking lander and by Ivanov<sup>7</sup> to describe Soyuz aerodynamics. Both these studies found that the drag coefficient could be given as a function of the logarithm of the Knudsen number. Curve fits 1 and 2 are in qualitative agreement with the results of

Wilmoth and Ivanov. It is worth noting the anomaly around  $10^{-8}$  kg/m<sup>3</sup>, where the rate of decrease of the drag coefficient decreases. The investigation of the cases with density greater than  $10^{-8}$  kg/m<sup>3</sup> continues, but it is currently believed that the anomaly is due to the change over from the free-molecular regime to the transition regime. More specifically, the shock layer upstream of the vehicle becomes less diffuse and changes the drag characteristics of the vehicle (Hoerner<sup>8</sup>).

## VI. Conclusions

A three-dimensional aerothermal analysis of the Mars Reconnaissance Orbiter (MRO) was conducted using the Direct Simulation Monte Carlo (DSMC) method of Bird. The analysis indicates that the main parameters influencing the heat flux to the vehicle are the angle of attack and the thermal accommodation coefficient. The wall temperature was not found to influence the heat flux significantly. A correlation for the drag coefficient as a function of the density was developed. However, the accuracy of these predictions ultimately depends on accurate knowledge of chemical reaction and surface accommodation data.

Future work will aim at improving understanding of the drag characteristics of the MRO. The physical phenomena behind the anomaly that was observed need to be better understood. That could lead to better future spacecraft designs. A more detailed design of the MRO will also have to be studied. Having herein identified the main parameters that affect the results, the analysis can be focused on these only.

## Acknowledgments

The authors would like to recognize the hard work and dedication from everyone involved with the Mars Reconnaissance Orbiter Program. This work was supported by the Mars Reconnaissance Orbiter Program, under contract to the Jet Propulsion Laboratory, contract number 1234906. We would also like to specifically recognize the efforts of Pete Huseman at LMA for facilitating the cooperation between LMA and Sandia National Labs, John Vandermeer at LMA for generating the CAD model used as the basis for this analysis, and Cynthia Camp at LMA for her work in generating the surface grid models.

The authors also gratefully acknowledge useful discussions and comments on the manuscript by Basil Hassan (SNL), Ryan Bond (SNL) and Martin D. Johnston (NASA/JPL).

## References

1. Lee, S.W., Skulsky, E.D., Chapel, J., Cwynar, D., Gehling, R., 2003, "Mars Reconnaissance Orbiter Design Approach for High-Resolution Surface Imaging", AAS 03-067, 26th Annual AAS Guidance and Control Conference, Feb. 5-9, Breckenridge, CO.
2. Bird, G.A. 1994, *Molecular Gas Dynamics and the Direct Simulation of Gases*, Oxford University Press.
3. LeBeau, G.J., 1999, "A Parallel Implementation of Direct Simulation Monte Carlo Method", *Computer Methods and Applied Mechanics and Engineering*, Vol. 174, pp. 319-337.
4. Park, C. 1994, *Nonequilibrium Hypersonic Aerothermodynamics*, Willey & Sons.
5. Gallis, M.A., Harvey, J.K., 1998, "On the Modeling of Thermochemical Non-Equilibrium in Particle Simulations", *Physics of Fluids*, Vol. 10, No 6., pp. 1344-1358.
6. Wilmoth, R.G., Blanchard, R.C., Moss, J.N., 1999, "Rarefied Transitional Bridging of Blunt Body Aerodynamics", *Rarefied Gas Dynamics*, Ed. Brun, R., Campargue, R., Gatinol, R., Lengrand, J.-C., Vol.2, pp.609-616, Cepadues Editions.
7. Ivanov, M.S., Markelov, G.N., Gimelshein, S.F. Mishina, L.V. Krylov, A.N, Greckho, N.V., 1998, "High Altitude Capsule Aerodynamics with Real Gas Effects", *J. of Spacecraft and Rockets*, Vol.35. No. 1., pp.16-22.
8. Hoerner, S.F., 1965, *Fluid Dynamic Drag*.

## Appendix 1

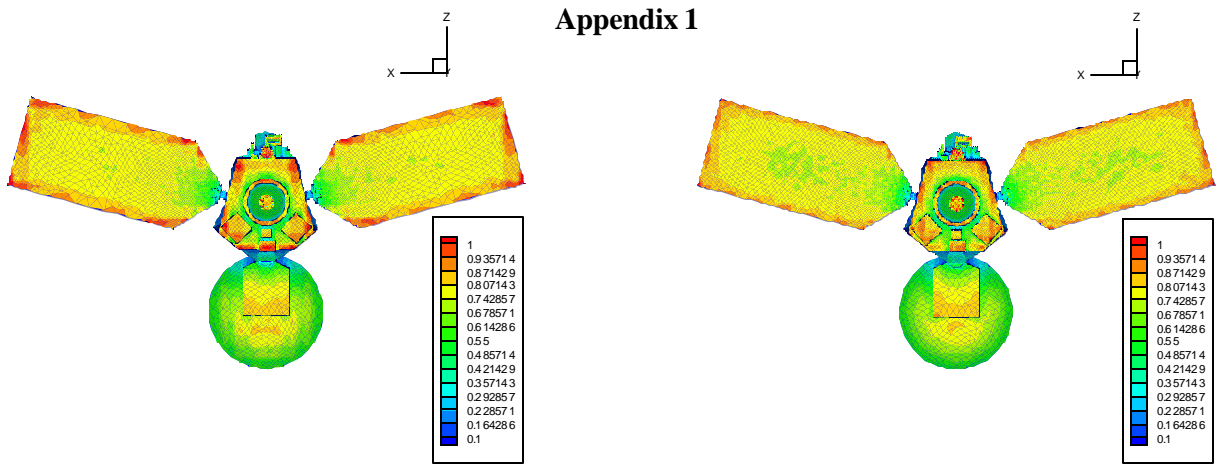


Figure A1.  $C_h$  for case 1 of Table 1.

Figure A4.  $C_h$  for case 4 of Table 1.

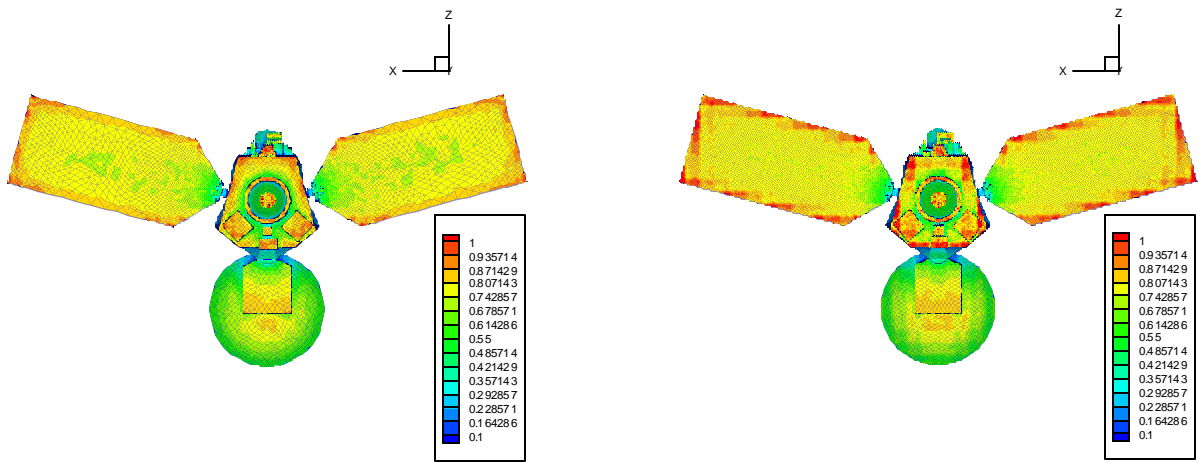


Figure A2.  $C_h$  for case 2 of Table 1.

Figure A5.  $C_h$  for case 5 of Table 1.

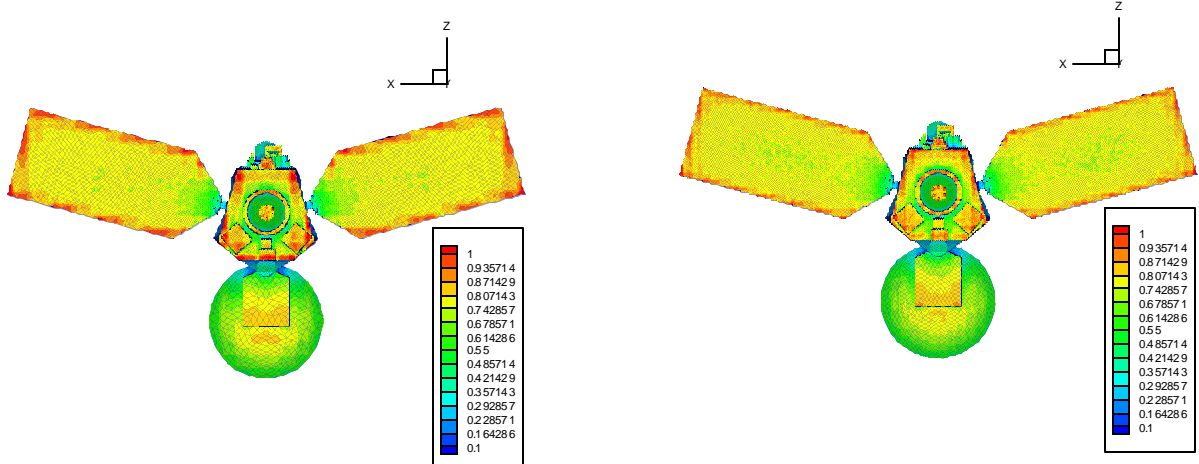


Figure A3.  $C_h$  for case 3 of Table 1.

Figure A6.  $C_h$  for case 6 of Table 1.